

# Understanding of intriguing metal to semiconductor transition in $\text{Ni}_{0.5}\text{Zn}_{0.5}\text{Fe}_2\text{O}_4$ nanoparticulates

Pooja Y. Raval<sup>1</sup>, Shrey K. Modi<sup>2</sup>, Khayati G. Vyas<sup>3</sup>, Priya L. Mange<sup>3</sup>, Kunal B. Modi<sup>3,\*</sup>

<sup>1</sup>Department of Physics, Harivandna College, Munjka, Rajkot 360005, India

<sup>2</sup>Department of Civil Engineering, Government Engineering College, Rajkot 360007, India

<sup>3</sup>Department of Physics, Saurashtra University, Rajkot 360005, India

\*Corresponding author: E-mail: kunalbmodi2003@yahoo.com

DOI: 10.5185/amlett.2021.031614

Temperature-dependent electrical transport characteristics of un-milled and high-energy ball-milled samples (3 h (70 nm), 6 h (55 nm) and 9 h (45 nm)) of  $\text{Ni}_{0.5}\text{Zn}_{0.5}\text{Fe}_2\text{O}_4$  spinel ferrite were explored. A well-defined metal to semiconductor transition exhibited by all the samples has been construed in view of direct and superexchange cationic interactions and delocalization to localization of charge carriers on increasing temperature. The peak temperature ( $T_{\text{max}}$ ) was found to shift towards a higher temperature side on milling principally governed by the lattice vibration scattering and intrinsic excitation. The crystallite size reduction, enhancement in strain and sudden decrease in the formation and octahedral site occupancy of  $\text{Fe}^{2+}$  ions on milling found responsible for the prodigious rise (~ 250 times) in normalized resistivity values for the sample comminuted for 9 h. The spectrum of energies corresponds to charge trapping centers that cause small bump (3 h milled sample) and sharp cusp (9 h milled sample) for  $T > T_{\text{max}}$ . These materials may be found suitable for thermal cutoff switching applications.

## Introduction

Synthesis and characterization of nanoparticles of wide-ranging materials are subject of curiosity since long from the aspects of basic understanding and put it into the applications. Nanoparticles demonstrate unusual, novel and improved physical properties when compared with bulk counterparts and that is the main motivation of nanoparticle research. The electrical conduction is chiefly governed by the preparative parameters. The soft chemical routes (bottom-up approaches) and high energy ball milling (top-down approach) are the principal routes of nanoparticles preparation. The production of the large quantity of nanocrystalline materials is referred to as the main advantage and the problem of contamination at least for some materials is often quoted as the main disadvantage to dismiss mechanical – attrition ball milling technique. In the beginning, the performance of the milling process was evaluated based on alteration in grain morphology. Nowadays it is a clear and well-established fact that in order to characterize nanopowders fully, mechanical milling induced stress and strain, as well as corresponding changes in structural parameters, must be taken into consideration [1-2].

The spinel ferrites being a ferrimagnetic material and poor conductors of electricity exhibit typical semiconducting characteristics in resistivity against temperature plots without or with a change in slope in the vicinity to magnetic ordering transition temperature [3-6]. We refer to some research reports, interestingly, few coarse-grained and nanostructured spinel ferrites are shown to exhibit unusual metal to semiconductor or semiconductor to metal like electrical transition dependent

on temperature [7-24]. According to an excellent review article by Imada *et. al.*, [25], metal-to-insulator transitions are attended by extremely large resistivity alterations by the orders of tens or so and extensively noticed in condensed-matter systems. This phenomenon of interest has been elucidated referring to various mechanisms and structural, microstructural parameters like change in grain size, band structure deformation, cation distribution, cationic interactions, canting angle, stress, strain, etc. It is worth mentioning that in literature pressure-induced [26,27], film thickness dependent [28,29], hydrogen doping induced [30], strain-stress induced [31-33], particle size induced [34], scalable light-induced [35], laser-induced [36] and orbital-order induced [37] metal to semiconductor transition has also been reported for other class of materials including spinel structured ferrites.

In this connection, a little while ago we have investigated structural properties modifications [1], X-ray Debye temperature [38] and optical, elastic and thermodynamical properties [39] of as-prepared (un-milled) and mechanically milled nanostructured spinel ferrite composition,  $\text{Ni}_{0.5}\text{Zn}_{0.5}\text{Fe}_2\text{O}_4$ . The important findings are summarized below to facilitate the discussion on the electrical property. All the samples have expected stoichiometry and possess a mono-phasic *fcc* spinel structure. The crystallite size ( $D$ ) decreases and atomic level strain ( $\langle \varepsilon^2 \rangle^{1/2}$ ) increases on milling duration. The unit cell parameter ( $a(\text{\AA})$ ) increase up to 6 h of milling and then shows a sudden decrease for 9 h milled sample (Table 1). Further, it is found that for all the samples about 60 % of  $\text{Zn}^{2+}$  ions reside at the octahedral (B-) sites though  $\text{Zn}^{2+}$  ions are known to possess the tetrahedral (A-) interstitial sites in *fcc* structure. The high energy milling

leads to two interesting phenomena of “temperature diffuse scattering” and “preferred orientation of grains” [1]. The captivating out-come prompted us to conduct an electrical property study on  $\text{Ni}_{0.5}\text{Zn}_{0.5}\text{Fe}_2\text{O}_4$  and establish the structure-property relationship in these ferrites. The observed signatures of resistivity against temperature plots including a transition from an anomalously large positive temperature coefficient to a negative temperature coefficient of electric conduction have been discussed based on various aspects. The prodigious relative resistivity value ( $\sim 250$ ) for 9 h milled sample of  $\text{Ni}_{0.5}\text{Zn}_{0.5}\text{Fe}_2\text{O}_4$ , the highest ever reported for any materials in general and spinel structured ferrites in particular, is subject of great attention. It is quite relevant to mention that the electrical conductivity of nanocrystalline (grain size 14-63 nm)  $\text{Ni}_{0.5}\text{Zn}_{0.5}\text{Fe}_2\text{O}_4$  spinel samples prepared by high energy mechanical milling process (similar to that employed in the present study) exhibit conventional semiconducting behavior with the change in slope at the temperature corresponds to Neel temperature of the samples [3].

### Experimental details

The experimental particulars in relation to the synthesis of polycrystalline spinel ferrite composition,  $\text{Ni}_{0.5}\text{Zn}_{0.5}\text{Fe}_2\text{O}_4$ , using standard two-steps sintering method (un-milled sample), preparation of nanostructured, 3 h, 6 h and 9 h milled samples by the ball-milling process, chemical stoichiometry verification by energy-dispersive analysis of X-ray spectroscopy, particle morphology investigation by means of transmission electron microscopy and phase formation study as well as structural parameters ascertainment by a detailed examination of X-ray diffraction line profiles are given in [1,38-39]. The  $\text{Ni}_{0.5}\text{Zn}_{0.5}\text{Fe}_2\text{O}_4$  spinel ferrite composition synthesized by usual double sintering ceramic technique [1] (un-milled sample) was milled for 3 h, 6 h and 9 h duration using Fritsch, Germany, made high energy planetary ball mill (pulverisette 6) with tungsten-carbide (W-C) vial and balls. The balls to powder weight ratio of 8:1 were maintained and milling intensity was kept 600 revolutions per minute. Water was added to the container to improve particle mobility during the milling process.

The cylindrically pelletized ferrite samples having an identical diameter of 1 cm and thickness varying from 0.2-0.3 cm were used for temperature-dependent direct current resistivity measurements. Both the surfaces of disc samples were burnished with fine sand paper, clean with mild hydrochloric acid and propanone. Eventually, graphite was applied on flat faces of the pellet on which thin aluminum foil was also retained for the non-rectifying electrical junction. The bi-terminal pressure contact technique was employed to measure the variation of resistance with temperature by keeping the sample holder in a horizontal electric furnace. The resistance was measured using a BPL meg-ohm meter and temperature by chromel- alumel thermal element. The electrical resistance was noted during the course of the cooling cycle at regular intervals of 20 °C.

### Results and discussion

The Rietveld fitted X-ray powder diffraction patterns executed by General Scattering Analysis Software for un-milled, 3 h, 6 h and 9 h milled samples of  $\text{Ni}_{0.5}\text{Zn}_{0.5}\text{Fe}_2\text{O}_4$  spinel structured ferrite composition are shown in Fig. 1. A painstaking structural analysis demonstrates that the samples are single phase compounds, crystallizing in the face-centered cubic (*fcc*) spinel structure of space group  $\text{O}_h^7 \text{Fd}3\text{m}$  [1]. The structural parameters, lattice constant,  $a$  (Å), X-ray density ( $\rho_x$ ) [39], bulk density ( $\rho$ ) [1] and porosity ( $P$  (%)), values for all the samples have been included in Table 1 to facilitate the further discussion.

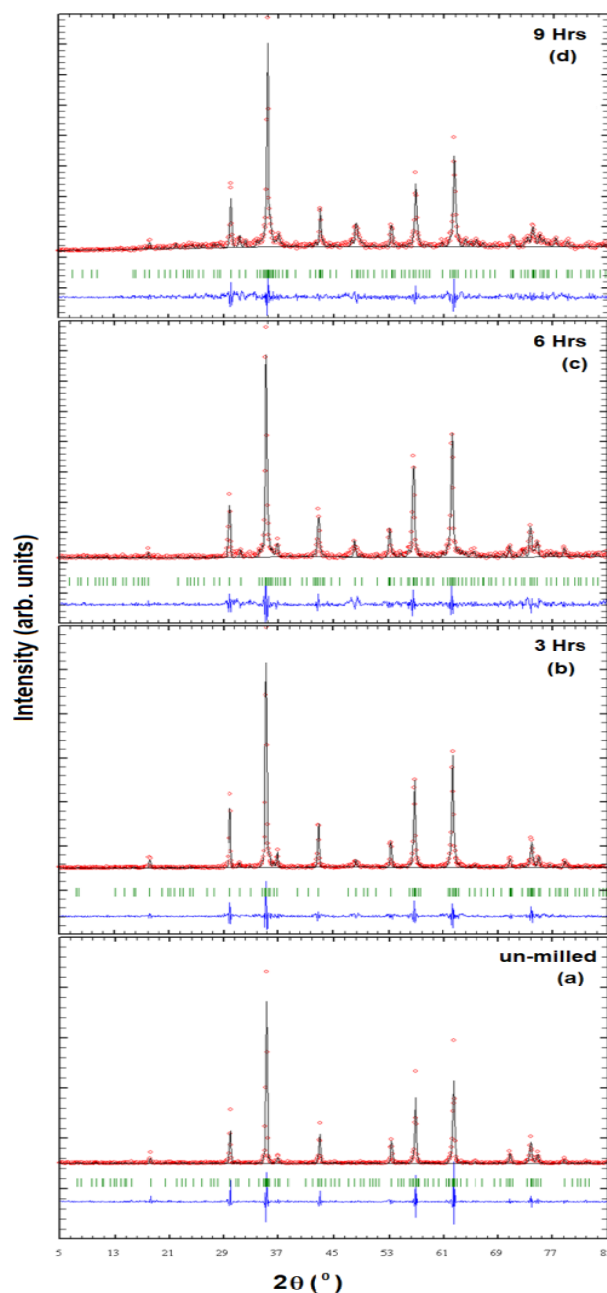
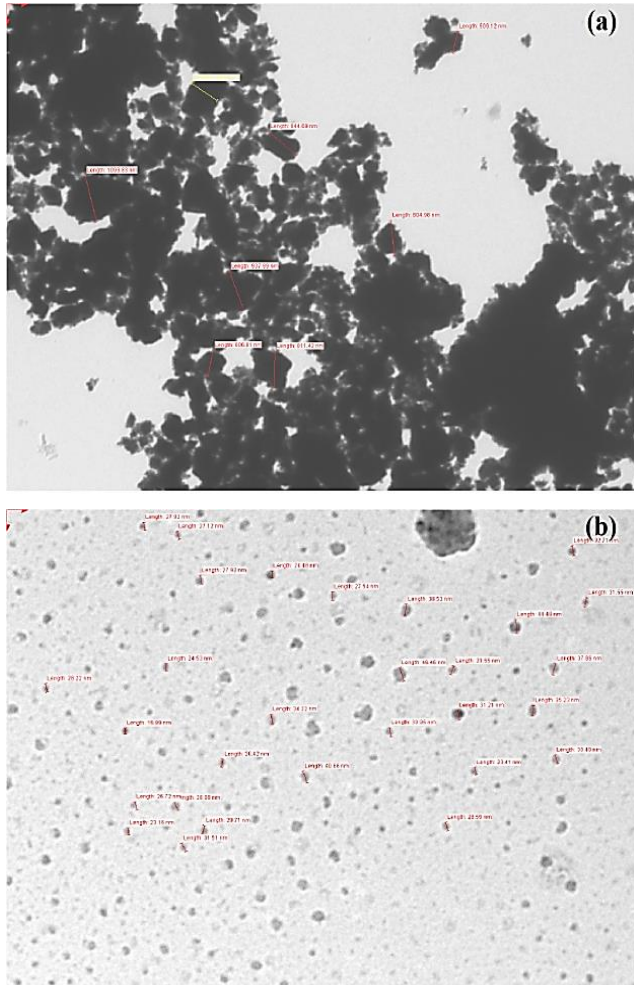


Fig. 1. Rietveld fitted X-ray powder diffraction patterns for un-milled (a), 3 h (b), 6 h (c) and 9 h (d) milled samples of  $\text{Ni}_{0.5}\text{Zn}_{0.5}\text{Fe}_2\text{O}_4$  ferrite composition recorded at 300 K.



**Fig. 2.** Transmission electron micrographs (a) un-milled sample (b) ultrasonicated particles for 9 h milled sample.

Typical transmission electron micrographs (TEM) for an un-milled and 9 h milled samples of  $\text{Ni}_{0.5}\text{Zn}_{0.5}\text{Fe}_2\text{O}_4$  ferrite are displayed in **Fig. 2(a)** and **Fig. 2(b)**. Owing to the ferrimagnetic nature of the samples an assemblage of particles is observed (**Fig. 2(a)**) thus the reliable particle size determination may not be possible. TEM of ultrasonicated 9 h milled sample has confirmed an average particle size of 30 nm (**Fig. 2(b)**) while for an un-milled sample (not shown) it was found to be  $\sim 900$  nm. The particle sizes estimated are consistent with the crystallite sizes ( $D$ ) estimated based on FWHM of the X-ray diffraction line profiles [1] (**Table 1**).

**Table 1.** Structural, microstructural and electrical parameters for nanostructured  $\text{Ni}_{0.5}\text{Zn}_{0.5}\text{Fe}_2\text{O}_4$  spinel ferrite composition.

Milling Duration (h)	$a(\text{\AA}) \pm 0.002\text{\AA}$	$\rho_x (\text{g/cm}^3)$	$\rho (\text{g/cm}^3)$	$P$ (%)	$T_{\text{max}} (\text{K}) \pm 2 \text{ K}$	$\langle \sigma^2 \rangle^{1/2} \times 10^{-5}$	$D$ (nm) $\pm 2 \text{ nm}$	$L(\text{\AA})$
0	8.425	5.283	4.53	14.25	423	-	1000	2.979
3	8.429	5.276	4.50	14.71	450	7.07	70	2.980
6	8.439	5.257	4.37	16.87	459	22.62	55	2.984
9	8.414	5.304	4.38	17.42	476	30.40	45	2.975

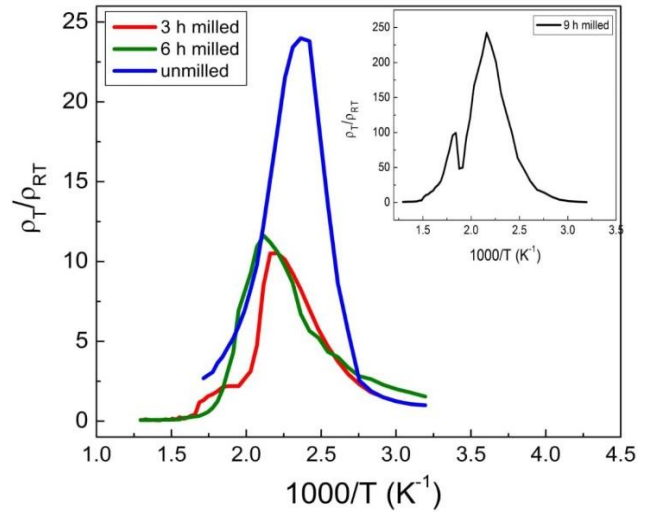


**Fig. 3.** Variation of normalized resistivity as a function of reciprocal of temperature for un-milled, 3h, 6h and 9h milled samples of  $\text{Ni}_{0.5}\text{Zn}_{0.5}\text{Fe}_2\text{O}_4$  spinel ferrite composition.

**Fig. 3** displays the normalized resistivity,  $\rho_T/\rho_{\text{RT}}$ , against reciprocal of temperature ( $1000/T$ ) plots for un-milled and milled samples of  $\text{Ni}_{0.5}\text{Zn}_{0.5}\text{Fe}_2\text{O}_4$ . All the ferrites demonstrate a sharp cusp ( $T_{\text{max}}$ ) correspond to metallic ( $T < T_{\text{max}}$ ) to semiconductor ( $T > T_{\text{max}}$ ) type electrical transition. According to classic work of Goodenough [40] when strong cation-cation interactions (direct exchange interactions) dominate in the system electrical conductivity is metallic in nature as a function of temperature and may become semiconductor at a much lower temperature. Conversely, if cation-anion-cation interactions (superexchange interactions) or weak direct magnetic interactions dominate, the system may show semiconducting or insulating type electrical conductivity characteristics with increasing temperature. If the metallic cations residing on the B-sites have outer electron configuration  $3d^m$  where  $4 \leq m \leq 8$  ( $e_g$  levels degenerate), the superexchange magnetic interactions need to be predominant, and nevertheless for  $m \leq 3$ , the direct interactions would be strengthened as compared to the superexchange interactions. In the present composition, both the magnetic cations,  $\text{Ni}^{2+}$  ( $2 \mu_B$ ) and  $\text{Fe}^{3+}$  ( $5 \mu_B$ ), taking part in the conduction process have electronic configuration,  $3d^8$  and  $3d^5$ , respectively, lie in the range,  $4 \leq m \leq 8$ . Thus, among the superexchange interactions and feeble direct interactions, former interactions will be ascendant in the investigated samples. Also, the existence of metallic cations in different oxidation states gives rise to the metallic character. This concept explains metallic to semiconductor transition in many ferrite materials. Thus, based on the above discussion for  $T < T_{\text{max}}$ , metallic type conduction, the direct magnetic interactions among  $\text{Fe}^{3+} - \text{Fe}^{3+} / \text{Fe}^{2+}$  and  $\text{Ni}^{2+} - \text{Ni}^{2+} / \text{Ni}^{3+}$  are stronger over  $\text{Fe}^{3+} - \text{O}^{2-} - \text{Fe}^{3+} / \text{Fe}^{2+}$  and  $\text{Ni}^{2+} - \text{O}^{2-} - \text{Ni}^{2+} / \text{Ni}^{3+}$  interactions. For  $T > T_{\text{max}}$  semiconducting like conduction is caused by the dominance of  $\text{Fe}^{3+}(\text{ferric}) - \text{O}^{2-} - \text{Fe}^{3+} / \text{Fe}^{2+}$  (ferrous) and  $\text{Ni}^{2+} - \text{O}^{2-} - \text{Ni}^{2+} / \text{Ni}^{3+}$  interactions. Based on

the crystal field and ligand field theories [13], it is established that the splitting of  $3d$  level of  $\text{Ni}^{2+}$ , is  $10 D_q$ , while for ferric ion ( $\text{Fe}^{3+}$ ) it is zero. This implies  $\text{Ni}^{2+}$ -  $\text{O}^{2-}$  -  $\text{Ni}^{2+}$  interactions are the most prominent at the B-sites of the compounds.

In ferrite materials, the mechanism responsible for electrical transport can be explained considering the potential on grain boundary ( $\phi$ ) and  $e_g$  electron energy ( $E_K$ ). Usually, the transport mechanism emerges through the hopping of localized  $d$ - electrons amongst valance distributions of metallic cations on the octahedral complexes. The cation  $3d$  level splits into less stable doubly degenerate  $e_g$  electrons and more stable triply degenerate  $t_{2g}$  electrons owing to the electrostatic interaction among anion and cation electrons. If  $E_K > e\phi$ , the electrons will be delocalized and proactively involved in the conduction mechanism but when  $E_K < e\phi$  the  $e_g$  electrons will be localized. In the temperature range,  $T < T_{\max}$ ,  $E_K > e\phi$ , where delocalization of charge carriers and orientations of spin induce conducting channels in the form of  $[\text{Fe}^{3+} - \text{Fe}^{2+}]$  and  $[\text{Ni}^{2+} - \text{Ni}^{3+}]$  links. These channels engender the delocalized of the electrons which improve the mobility of charge carriers and thus metallic behavior is noticed [7]. For  $T > T_{\max}$ , these delocalized electrons ( $e_g$  electrons) begin to be localized in the existence of magnetic disorder (i.e. disorientation of the surface and core spins) and non-magnetic disorder (i.e. electronic trap center) satisfying the condition of  $E_K < e\phi$ . Thus, the jumping possibility of the  $e_g$  electrons enhances thereby reducing the resistance of the samples that result in semiconducting behavior. According to Anderson [41], if the right triangle is formed between cation-anion-cation, these interactions are weak and direct interactions become predominant. Nevertheless, when that angle becomes a straight angle or obtuse angle of  $120^\circ$ , then superexchange magnetic interactions are incomparable.

The metal-like conduction observed in the temperature range of  $300\text{-}465 \pm 15$  K in  $\text{Ni}_{0.5}\text{Zn}_{0.5}\text{Fe}_2\text{O}_4$  nanoparticulates can also be explain based on the deformation of band structure at the edges of valance band and conduction band. In the semiconducting region ( $T > T_{\max}$ ), resistivity is a function of density and mobility of charge carriers and that decreases on lowering of temperature. For  $T < T_{\max}$  (metal-like state) charge carrier density keeps decreasing but charge carrier mobility increases. In low-temperature semiconducting regions ( $T \ll T_{\max}$ ) as pointout by Goodenough [40] both mobility and number of charge carriers are trapped in localized states [1].

Another one riveting fact is that for the majority of spinel ferrites metal-like conductivity is observed in the temperature range of  $300\text{-}400$  K and corresponding excitation energy needed is  $25\text{-}35$  meV. This energy span is comparable with the magnetic exchange energy necessary for the electronic spins recombination amongst  $e_g$  and  $t_{2g}$  states all along with the cationic rearrangement

amongst the A- and B- sites or hoping of charge at the B-sites of the spinel lattice. Beyond this temperature range for  $T < T_{\max}$  and  $T \gg T_{\max}$  (semiconducting regions) the temperature-activated process take over the conduction owing to delocalization of charges influenced by the magnetic exchange interactions as well as reordering of spins in  $t_{2g}$  and  $e_g$  electronic energy levels of magnetic cations residing at the octahedrally coordinated complexes.

It is found that the lattice parameter  $a(\text{\AA})$  enhances for an un-milled sample ( $8.425 \text{\AA}$ ) to 6 h milled sample ( $8.439 \text{\AA}$ ) and suddenly reduces for 9 h milled sample ( $8.414 \text{\AA}$ ) [1] (Table 1). We have correlated the jump length or hoping length ( $L = 1.4142(a) / 4$ ) [42] of the charge carriers among ferrous and ferric ions (conduction owing to electrons) and  $\text{Ni}^{2+}$  and  $\text{Ni}^{3+}$  (conduction due to holes) on the B-site with the electrical resistivity. Accordingly, with an increase in  $a$  ( $\text{\AA}$ ) increase in  $L$  with milling time is expected. This insinuates that charge carriers required an excessive amount of energy to hop from one cationic site to another that curtails the hopping responsible for conduction in the system with an increasing milling period as observed. Long back single-crystalline lithium vanadate spinels,  $\text{LiV}_2\text{O}_4$ , have shown temperature-dependent metallic conductivity and have been described on the basis of separation among two neighboring vanadium ion at the octahedral site [43]. Along the same line, for  $T < T_{\max}$  separation distance among Fe-Fe ion is less than a specific threshold value where in addition to the hopping of electron a nearly band-like conductivity intervenes, characterized by the observed metal-like conductivity behavior. As soon as sample temperature  $T > T_{\max}$  separation between Fe-Fe ions enhances to beyond the threshold value owing to thermal enlargement of the unit cell. This hinders the band-like conduction and once again conduction mechanism gets dominated by electron hopping amongst the neighboring B-sites. Thus, the typical thermal characteristics noticed for  $T > T_{\max}$  are ascribed to the electron hopping mechanism.

It is perceived that for the entire range of temperature normalized resistivity values increase with milling duration. This may be ascribed to the grain size reduction effect. The highly resistive grain boundary (GB) volume increases as compared to the volume of grains on grain size reduction. The GBs are the regimes of mismatching among the energy states of adjoining grains and as a consequence the corresponding impedance to the stream of charge carriers increases. An additional benefit of tiny grains is that it assists in diminishing ferrous ions ( $\text{Fe}^{2+}$ ) as oxygen moves swiftly the smaller regions, thus maintaining Fe ions in +3 states. Provided electron average free path is larger than the crystallite size, scattering owing to the grain boundary dominates and the temperature coefficient of resistance of materials also increases [44].

The metal to semiconductor transition temperature shifted to higher temperatures with milling (**Fig. 3**). The sharp cusp temperature,  $T_{\max}$ , that separates the metallic conduction ( $T < T_{\max}$ ) and region of semiconductor ( $T > T_{\max}$ ) rely on the rivalry amongst the lattice vibration scattering and intrinsic excitation that increases on grain size reduction. Thus,  $T_{\max}$  increases with the increases of milling hours (**Table 1**). The results are consistent with the electrical behavior of Cu-Zn nanoferrites [11]. On the increasing temperature, the lattice vibration scattering effect gets enhanced that obstructs the electronic conduction but decreases the dc drift mobility correspond to the metallic conduction region. On the other hand, the ionization owing to impurity as well as intrinsic excitation are anticipated to enhance the charge carrier concentration and thus resistivity reduces in the semiconducting region on further increase in temperature. The Neel temperature ( $T_N$ ) for bulk  $\text{Ni}_{0.5}\text{Zn}_{0.5}\text{Fe}_2\text{O}_4$  ferrite composition is reported to be 538 K, while it is found to be 611 K (14 nm), 592 K (16 nm) and 573 K (50 nm) for nanostructured materials [3]. The transition temperatures ( $T_{\max}$ ) identified in the present study are far below than the recorded one, so it cannot be correlated with a magnetic ordering transition temperature ( $T_N$ ). Thus, it is concluded that magnetic ordering has no influence on the conduction process.

It has been shown by Duan *et al.*, [31] that volume expansion together with strain and stress can alter the density of charge carriers not only that to some extent the mobility of the charge carriers also. With the increase of strain the mobility of carriers decreases, thus resistivity is expected to increase. The RMS value of atomic level strain  $\langle \varepsilon^2 \rangle^{1/2}$  is found to increase with milling hours (Table 1). Because the strain is summative with time, at the beginning of the milling process it takes place on the surface region of grains. Notwithstanding as milling process get continuous, the grains become smaller and smaller and strain developed throughout the grain. In the case of  $\text{Ni}_{0.36}\text{Zn}_{0.64}\text{Fe}_2\text{O}_4$  nanoparticles synthesized by the mechanical alloying process for 30 h, Hajalilou *et al.*, [45] have shown that the resistivity has a direct correlation with porosity and an inverse correlation with grain size. On the same line of argument, it is now possible to explain the observed increase in the relative resistivity value with increasing milling duration from 3 h to 9 h in the light of porosity and grain size. As the porosity increases with milling (**Table 1**), the number of vacancies, scattering centers and voids for the electric charge carriers increases, causing a rise in resistivity. On the other hand, the small particles have a large surface to volume ratio which acts as a barrier to electron flow and thereby increases the resistivity. Thus, observed a huge rise in a maximum of normalized resistivity value for 9 h milled sample (**Fig. 3**) may be correlated with the cumulative effect of an increase in microstrain, increase in porosity and a decrease in grain size with the milling process. Noticeable sudden rise in normalized resistivity values for 9 h milled sample as compared to 3 h and 6 h milled samples may also be

correlated with an observed sudden decrease in lattice constant value for 9 h milled sample as compared to unmilled, 3 h and 6 h milled samples (**Table 1**)[1]. The reduction in the value of the cell edge parameter suggests less formation of larger ferrous ion ( $\text{Fe}^{2+}$ ) (0.74 Å) from ferric ion ( $\text{Fe}^{3+}$ ) with an ionic radius of 0.645 Å in 9 h milled sample as compared to 3 h and 6 h milled samples. That decreases the number of  $\text{Fe}^{3+}\text{-Fe}^{2+}$  pairs at the octahedral interstices, and thus resistivity abruptly increases as observed. On the same line of argument observed reduction in normalized resistivity values for 3 h and 6 h milled samples as compared to an unmilled sample can be explained.

It is worthwhile to notice the appearance of a broad bump for a 3 h milled sample (centered at 570 K) and a sharp peak (centered at 536 K) for 9 h milled sample for  $T > T_{\max}$  (**Fig. 3**). In this regime decrease in normalized resistivity is owing to the enhancement in the density of mobile charge carriers, along with charge carriers escape from their trapping centers with increasing temperature. The range of energy rather a single value is required to persist these trapped charges. The small hump and intense peak are thus in consequence of these aggregate values of energies [7]. The thermal variation of direct current resistivity characteristics resembles the suitability of these materials for thermal switching applications. Further work is in progress.

## Conclusions

The relative strength of direct and superexchange magnetic interactions at the octahedral complexes, as well as potential on grain boundary and  $e_g$  electron energy, are responsible for metal to semiconductor type electrical transition as a function of temperature in nanostructured  $\text{Ni}_{0.5}\text{Zn}_{0.5}\text{Fe}_2\text{O}_4$  spinel ferrites. Observed small bump (3 h milled sample) and sharp peak (9 h milled sample) at high temperatures are mainly due to a spectrum of energies correspond to charge trapping centers. The gigantic rise (~ 250 times) in normalized resistivity values manifested by 9 h milled sample is owing to the cumulative effect of grain size reduction, strain enhancement and reduced formation of ferrous ions residing on the octahedral sites on milling. The shifting of transition temperature towards a higher temperature on milling is due to rivalry amongst the lattice vibration scattering and intrinsic excitation.

## Acknowledgments

The research fellowship sanctioned to Ms. Priya L. Mange under the INSPIRE scheme of DST-New Delhi, India is highly appreciated (IF 190111).

## Conflict of Interest

The authors declare that they have no conflict of interest.

## Keywords

Spinel ferrite, mechanical milling, nanoparticles, electrical property, metal to semiconductor transition, cationic interactions, structural and microstructural parameters.

Received: 23 July 2020

Revised: 27 August 2020

Accepted: 01 September 2020

## References

1. Vasoya, N. H.; Vanpariya, L. H.; Sakariya, P. N.; Timpbadiya, M. D.; Pathak, T. K.; Lakhani, V. K.; Modi, K. B.; *Ceram. Int.*, **2011**, 36, 947.
2. Modi, K.B.; Dolia, S.N.; Sharma, P.U.; *Ind. J.Phys.*, **2015**, 89, 425.
3. Sivakumar, N.; Narayanasamy, A.; Ponpandian, N.; Greneche, J.M.; Shinoda, K.; Jeyadevan, B.; Tohji, K.; *J. Phys. D : Appl. Phys.*, **2006**, 39, 4688.
4. Chhaya, S. D.; Pandya, M. P.; Chhantbar, M. C.; Modi, K. B.; Baldha, G. J.; Joshi, H. H.; *J. Alloy. Compd.*, **2004**, 377, 155.
5. Lakhani, V. K.; Modi, K. B.; *J. Phys. D: Appl. Phys.*, **2011**, 11, 245403.
6. Hussain, K.; Bibi, A.; Jabeen, F.; Amin, N.; Mahmood, K.; Ali, A.; Iqbal, M.Z.; Arshad, M.I.; *Physica B : Cond. Matter*, **2020**, 584, 412078.
7. Pandya, R. J.; Sengunthar, P.; Zinzuvadiya, S.; Joshi, U.S.; *Appl. Phys. A*, **2019**, 125, 614.
8. Bhowmik, R. N.; Kumar, K. S. A.; *Mater. Chem. Phys.*, **2016**, 177, 417.
9. Bhowmik, R.N.; Vijayasri, G.; *J. Appl. Phys.*, **2013**, 114, 223701.
10. Kumar, S.; Munjal, S.; Khare, N.; *J. Phys. Chem. Solids.*, **2017**, 105, 86.
11. Li, Le-Z.; Peng, L.; Zhung, X-X; Wang, R.; Tu, X-Q.; *J. Magn. Magn. Mater.* **2016**, 419, 407.
12. Younas, M.; Nadeem, M.; Atif, M.; Grossinger, R.; *J. Appl. Phys.*, **2011**, 109, 093704.
13. Ata-Allah, S. S.; Kaiser, M.; *Phys. Stat. Sol. (a)*, **2004**, 201, 3157.
14. Chhaya, U.V; Kulkarni, R.G.; *Mater. Lett.*, **1999**, 39, 91.
15. Godbole, B.; Badera, N.; Shrivastava, S.B.; Jain, D.; Sharath Chandra, L.S.; Ganesan, V.; *Phys. Proc.*, **2013**, 49, 58.
16. Rao, B.P.; Rao, K.H.; Rao, T.V.; Paduroru, A.; Caltum, O.F.; *J. Opt. Adv. Mater.*, **2005**, 7, 701.
17. Bhowmik, R.N.; *Mater. Res. Exp.*, **2014**, 1, 015903.
18. Baruwati, B.; Rana, R.K.; Manorama, S.V.; *J. Appl. Phys.*, **2007**, 101, 014302.
19. Ashiq, M.N.; Ehsan, M.F.; Iqbal, M.J.; Gul, I.H.; *J. Alloy. Compd.*, **2011**, 509, 5119.
20. Kannan, R.; Rajagopan, S.; Arunkumar, A.; Vanidha, D.; Murugaraj, R.; *J. Appl. Phys.*, **2012**, 112, 063926.
21. Chauhan, L.; Sreenivas, K.; *Adv. Sci. Lett.*, **2016**, 22, 3857.
22. Nazir, M.A.; Islam, M.Ul.; Ali, I.; Ali, H.; Shahid., B.A.; *J. Elect. Mater.*, **2016**, 45, 1065.
23. Li, Le-Z.; Zhong, X-X.; Wang, R.; Tu, X-Q.; He, L.; *J. Mater. Sci.: Mater. Elect.*, **2018**, 29, 7233.
24. Modi, K.B.; Joshi, H.H.; Kulkarni, R.G.; *J. Mater. Sci.*, **1996**, 31, 1311.
25. Imada, M.; Fujimori, A.; Tokura, Y.; *Rev. Mod. Phys.*, **1998**, 70, 1039.
26. Matsuoka, T.; Shimizu, K.; *Nature*, **2009**, 458, 186.
27. Rahman, S.; Samanta, S.; Errandonea, D.; Yan, S.; Yang, K.; Lu, J.; Wang, L.; *Phys. Rev. B.*, **2017**, 95, 024107-1.
28. Kumar, A.; Maurya, S.; Chawla, S.; Patwardhan, S.; Kavaipatti, B.; *Appl. Phys. Lett.*, **2019**, 114, 212103.
29. Ciarrocchi, A.; Avsar, A.; Ovchinnikov, D.; Kis, A.; *Nature Commun.*, **2018**, 9, 1.
30. Yao, S.; Yoo, P.; Liao, P.; *Phys. Chem. Chem. Phys.*, **2019**, 21, 25397.
31. Duan, C-g.; Sabiryanov, R. F.; Liu, J.; Mei, W. N.; Dowben, P. A.; Hardy, J. R.; *Phys. Rev. Lett.*, **2005**, 94, 237201.
32. La Torre, A.; Botello-Mendez, A.; Baaziz, W.; Charlier, J-C.; Banhart, F.; *Nature Commun.*, **2015**, 6, 1.
33. Fang, H.; Wang, Ru-Zhi, Yan, Mi; Chen, Si-Ying; Wang, Bo; *Phys. Lett. A*, **2011**, 375, 1200.
34. Snow, A. W.; Wohltjen, H.; *Chem. Mater.*, **1998**, 10, 947.
35. Gomez, L. M.; Kumar, A.; Zhang, Yi; Ryu, K.; Badmaev, A.; Zhou, C.; *Nano let.*, **2009**, 9, 3592.
36. Andrew, R.; Leezma, M.; Lovato, M.; Wautelet, M.; Laude, L.D.; *Appl. Phys. Lett.*, **1979**, 35, 418.
37. Van Aken, B.B.; Jurchescu, O. D.; Meetsma, A.; Tomioka, Y.; Tokura, Y.; Palstra, T. M.; *Phys. Rev. Lett.*, **2003**, 90, 1.
38. Modi, K. B.; Pathak, T. K.; Vasoya, N. H.; Lakhani, V. K.; Baldha, G. J.; Jha, P. K.; *Ind. J.Phys.*, **2011**, 85, 411.
39. Modi, K. B.; Shah, S. J.; Pujara, N. B.; Pathak, T. K.; Vasoya, N. H.; Jhala, I. G.; *J. Mol. Stru.*, **2013**, 1049, 250.
40. Goodenough, J. B.; *Phys. Rev.*, **1960**, 117, 1442.
41. Anderson, P. W.; *Phys. Rev.*, **1959**, 115, 2.
42. Vasoya, N. H.; Lakhani, V. K.; Sharma, P. U.; Modi, K. B.; Kumar, Ravi; Joshi, H. H.; *J. Phys: Condens. Matter*, **2008**, 18, 8065.
43. Rogers, B.B.; Gillson, J.L.; Gier, T.E.; *Solid State Commun.*, **1967**, 5, 263.
44. Batoo, K. M.; Kumar, S.; Lee, C. G.; Alimuddin, *Current Appl. Phys.*, **2009**, 9, 1072.
45. Hajalilou, A.; Kamari, H. M.; Shamel, K.; *J. Alloy. Compd.*, **2017**, 708, 813.